MPM Coseismic Slope Runout Prediction Using the Intergranular Strain Anisotropy Hypoplastic Model

Abdelrahman Alsardi, M.Eng., S.M.ASCE[1]; Alba Yerro, Ph.D., M.ASCE[2]

[1]Graduate Student, Department of Civil and Environmental Engineering, Virginia Tech, Blacksburg, USA; e-mail: alsardi@vt.edu
[2]Assistant Professor, Department of Civil and Environmental Engineering, Virginia Tech, Blacksburg, USA; e-mail: ayerro@vt.edu

ABSTRACT

The Material Point Method (MPM) is an advanced particle-based numerical tool capable of modeling large deformations. However, its abilities to predict seismic site response, ground failure initiation, and post-failure consequences including undrained conditions, have not been fully realized. This research aims to use recent MPM developments to simulate earthquake-triggered slope failures. As a novelty, an advanced constitutive model such as the Intergranular Strain Anisotropy Hypoplastic model is implemented in an effective-stress undrained MPM framework to simulate the hydromechanical response of dense and loose sand. First, an MPM simulation of a level-ground sand column is used to understand the system-level undrained response under simple sinusoidal excitation. Loose sand tends to liquefy under an increase in pore pressure, while dense sand exhibits a decrease in pore pressure. Second, a small-scale slope geometry is adopted whereby the runout investigation is conducted using void ratios ranging from 0.45 to 0.95. The framework shows promising system-level results, needing further validation using centrifuge experiments.

INTRODUCTION

The occurrence of coseismic landslides poses significant risks on civil infrastructure and human lives. Empirical procedures, such as the Newmark-type regressions, often assume a viscoelastic site response, a simple sliding block model, and no significant generation of pore pressure that can cause liquefaction (e.g., Bray et al., 2018). Despite the emergence of advanced constitutive model concepts (e.g., bounding surface plasticity and hypoplasticity), conventional mesh-based numerical frameworks are yet incapable of simulating large deformation. This is mainly due to element geometry distortion, which renders negative element Jacobian with significant numerical drift. Over the past two decades, the numerical analysis community has been exploring particle-based techniques which either avoid the use of the computational mesh (e.g., SPH, RKPM, and DEM) or utilize dual mesh-particle domains (e.g., PFEM and MPM). Completely mesh-free techniques face challenges in tracking boundaries and applying boundary conditions, often requiring large computational cost and the use of 'ghost points'. In this work we adopt the Material Point Method (MPM) which is a hybrid numerical analysis tool that defines materials using Lagrangian points, each so-called a Material Point (MP), which move within a background Eulerian mesh (Sulsky et al., 1994). The background Eulerian mesh can be thought of as a

temporary scratch pad to solve the discretized governing equations before the numerical results are mapped back to the MPs. The background mesh does not store any information, and due to this, it can be moved or destroyed and regenerated after every time step.

The objective of this paper is to use the developed MPM framework proposed by Alsardi and Yerro (2023) together with an advanced hypoplastic constitutive model to simulate the large deformation behavior of sand under earthquake-triggered shaking. First, the advancements in MPM to simulate coseismic landslides are described, including a non-zero kinematic, periodic boundary conditions, and an explicit generalized-α time scheme. Second, the selected hypoplastic constitutive model (Fuentes and Triantafyllidis, 2015) is described along with its recent advances to simulate cyclic mobility (Fuentes et al., 2020). The element-level response under cyclic loading is described. Third, the framework is used to simulate 1D shaking in a 10 m high sand column considering different relative densities. The system-level response of the constitutive model is showcased using MPM in its capability to generate pore pressures in undrained conditions under cyclic loading. Finally, a theoretical slope geometry of an embankment is adopted, and a coseismic landslide runout is simulated for a range of initial void ratios.

BACKGROUND

The intergranular strain anisotropy hypoplastic (thereafter referred to as Hypo+ISA) constitutive model is implemented in the MPM framework. This section aims to provide a brief overview of the basis of the MPM and Hypo+ISA constitutive model along with recent improvements to simulate cyclic loading due to earthquakes.

MPM developments for earthquake applications: The explicit MPM (momentum formulation) algorithm involves the following steps in every timestep: (a) computing nodal external and internal forces by mapping the gradient of the stresses, (b) computing the nodal mass, (c) solving the momentum balance equation to compute nodal accelerations, (d) computing MP velocities and the strain field, (e) updating stresses using the selected constitutive model, (f) updating porosity, displacements and global positions, (g) and finally destroying all the nodal information and regenerating the mesh if necessary. The geotechnical engineering community has pioneered the application of MPM for multiphase simulation of soil. The drawbacks of the MPM include the increasing computational cost due to the back-and-forth mapping between the MPs and the background mesh. Also, the cell-crossing error when the MP passes from one element to another has practically not been eliminated due to the use of lower-order shape functions. In addition, a stiffening effect due to volumetric locking is present when simulating incompressible undrained behavior. Techniques to reduce or minimize these limitations include the use of mixed MP-Gauss point spatial integration, so-called “mixed-integration” (Al-Kafaji, 2013), time schemes that dissipate spurious high frequencies (Kontoe, 2006; Alsardi and Yerro, 2023), and pore pressure smoothing algorithms (Kularathna et al., 2021). In this work, a modified mixed-integration has been considered; while Gauss integration used to evaluate internal forces at the nodes of the computational mesh, the constitutive model is evaluated at each material point individually to keep track of state variables accurately.

The application of the MPM to simulate earthquake-triggered failure has been limited but gaining more attention in the past three years. A brief overview of the recent earthquake engineering research in MPM is summarized herein. Girigharan et al. (2020) employed a convective particle domain interpolation formulation to simulate liquefaction in a centrifuge using the UBCSAND constitutive model in MPM. Alsardi and Yerro (2021) introduced a simple MPM framework whereby a non-zero kinematic boundary condition is used to prescribe the earthquake motion on the nodes of the mesh. Additionally, they used a moving mesh technique by which the mesh follows the applied ground motion. Alsardi et al. (2021) validated the framework capabilities in reproducing a shaking table test on a clay embankment in a total stress analysis framework using a Tresca constitutive model considering an exponential strain softening law. A comparison was made with other mesh-based and Newmark-type techniques, and a good match was observed with MPM at small strains and assuming a simple elastoplastic behavior. Feng et al. (2021) extended the boundary conditions to simulate free field conditions for non-symmetric geometries in a double-point MPM formulation. Kohler et al. (2022) formulated a more generalized free-field implementation of boundary conditions and employed it to understand the post-shaking runout behavior using a von Mises model considering a linear strain-softening law. Alsardi and Yerro (2023) used periodic boundary conditions to better capture the resonant column frequencies, which was verified by comparing against the analytical transfer function solution assuming a simple linear elastic behavior. In addition, Alsardi and Yerro (2023) extended the explicit time integration scheme with an explicit Generalized-α algorithm to reduce the spurious oscillations that occur in the MPM analysis.

In this research, an effective stress single-point MPM undrained formulation is employed. The pore pressure increment, Δu, is estimated, as shown in Equation 1, as a function of the volumetric strain, ε_v, generated in the MP, bulk water modulus, K_w, and porosity, n.

$$\Delta u = \frac{K_w}{n}\varepsilon_v \tag{1}$$

It is well known that volumetric locking occurs when simulating undrained materials, particularly when using linear triangular elements. This results in a distorted pore pressure field in the MPM simulation which in turn affects the nodal acceleration solution. As such, a simple strategy is adopted herein where the stresses are mapped to the nodes and remapped to the MPs. This algorithm effectively smoothens the pore pressures, as demonstrated by Kularathna et al. (2021).

Constitutive modeling of sand under cyclic conditions: State-of-the-art literature in the MPM has rarely used an advanced constitutive model for the cyclic simulation of soils. Feng et al. (2021) employed MPM with a hypoplastic bounding surface constitutive model to simulate the earthquake-induced liquefaction of earthen dams. Kinematic hardening models are often most suitable to simulate the effects of cyclic loading on soils, as demonstrated by their element-level response (Wichtmann et al., 2019). These primarily include elastoplastic models such as Sanisand-type models (Dafalias and Manzari, 2004) and hypoplastic constitutive models (e.g., Hypo+ISA by Fuentes et al., 2020). This research focuses on the Hypo+ISA model due to its open-source UMAT availability, which has been incorporated in the authors' MPM code, an in-house version of Anura3D (www.Anura3d.com). The Hypo+ISA model was conceived by coupling the hypoplastic model of von Wolffersdorff (1996) with the theory of Intergranular Strain Anisotropy of Poblete et al. (2016) to enable the simulation of cyclic loading. This adds additional state

variables that enable the model to (a) reproduce the threshold strain amplitude dividing the elastic and plastic regime, (b) increase stiffness and reduce the often-overestimated plastic strain upon load reversal in hypoplastic models, and (c) include effects of cyclic mobility and ultimately liquefaction (i.e., zero mean effective stress). The model uses a yield surface, a hardening rule, and a bounding surface within the intergranular strain space in a critical state-compatible framework. The ISA constitutive equation presents the form in Equation 2, where m and y_h are scalar functions, $\overline{\mathrm{E}}$ and $\dot{\varepsilon}^p$ are called "mobilized" stiffness tensor and "mobilized" plastic strain rate, respectively.

$$\dot{\sigma} = m\overline{\mathrm{E}}\colon(\dot{\varepsilon} - y_h\dot{\varepsilon}^p) \tag{2}$$

The ISA equation is used with the conventional form of the hypoplastic model equation shown in Equation 3, where L^{hyp} is the 4th-order linear stiffness tensor and N^{hyp} is the 2nd-order nonlinear stiffness tensor (von Wolffersdorf, 1996).

$$\dot{\sigma} = \mathrm{L}^{hyp}\colon\dot{\varepsilon} + \mathrm{N}^{hyp}\left|\left|\dot{\varepsilon}\right|\right| \tag{3}$$

The UMAT implementation uses a sub-stepping scheme to iterate over small strain subincrements to achieve numerical convergence and consistency. However, this study does not address the accuracy of the constitutive model. Duque et al. (2022) highlighted several element-level limitations of Hypo+ISA. This includes stress undershooting, unrealistic one-way axial strain racheting, rapid pace of pore pressure generation, and inability to progressively reduce the shear stiffness at the liquefaction state.

1D RESPONSE OF A SAND COLUMN IN UNDRAINED CONDITIONS

A 10 m high column with a width of 1.25 m comprising 400 elements is generated with the aim of simulating free-field conditions in a level ground geometry. The non-zero kinematic boundary condition is used to apply the earthquake shear loading at the base of the column. Periodic boundary conditions are assigned to the lateral sides of the column to enable the simulation of the free field resonant modes. The mesh is moved in every timestep following the ground motion. The initial stresses are assumed with an at-rest lateral earth pressure coefficient of K_0=0.5. A sinusoidal wave is applied as a proxy to a cyclic reversing load of an earthquake (input acceleration $a = -0.02\cos(5t)$ and corresponding velocity $v = 0.1\sin(5t)$, where t is the overall real time).

The undrained effective stress formulation is employed herein with the calibrated parameters corresponding to Ottawa F65 sand used in the NSF-funded LEAP-2017 centrifuge testing program. The following are the Hypo+ISA material parameters obtained from the Ottawa F65 calibration by Fuentes et al. (2018): critical friction angle, ϕ_c'=32°; granular hardness, h_s=300 MPa; barotropy exponent, n_B=0.5; maximum void ratio, e_{i0}=0.850; critical void ratio, e_{c0}=0.785; minimal void ratio, e_{d0}=0.500; dilatancy exponent, α=0.1; density exponent, β=2.0; stiffness factor, m_R=3.5; IS yield surface radius, R=10^{-4}; IS hardening parameter, β_h=0.5; minimum value of χ, χ_0=4; control for the rate of accumulation of plastic strain, C_a=0.15; maximum value of χ, χ_{max}=15; cyclic mobility parameter, C_z=300. The implemented UMAT of Hypo+ISA constitutive model is validated herein using a stress-controlled cyclic triaxial incremental driver (Niemunis, 2008) and compared to laboratory experiments by Fuentes et al. (2018). Figures 1b and 2b show the stress paths we generated using Hypo+ISA constitutive model and the aforementioned

incremental driver. These compare satisfactorily to the cyclic triaxial results depicted in Figure 1c and 2c, respectively, performed on Ottawa F65 sand with an initial void ratio e=0.54.

Additional material properties adopted in the MPM model are: specific gravity, G_s=2.6, water density, ρ_w=1000 kg/m^3, and water bulk modulus, K_w=10^5 kPa. The simplified pore pressure smoothing algorithm was applied to mitigate stress oscillations due to volumetric locking consistent with Kularathna et al. (2021). For the dynamic calculation stage, the explicit generalized-α time scheme was activated with bifurcation spectral ratio ρ_b=0.818 consistent with Alsardi and Yerro (2023).

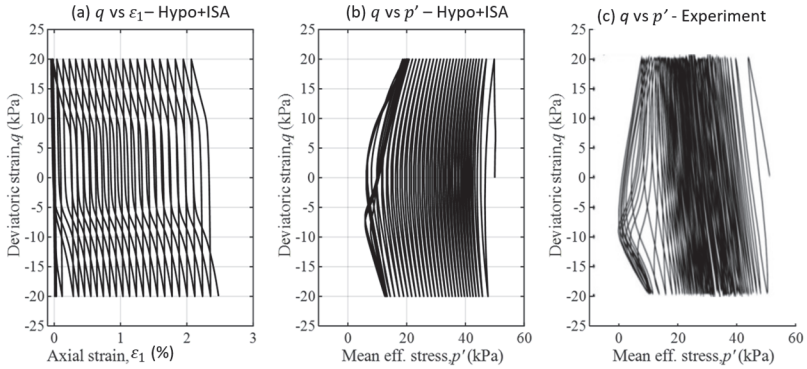

Figure 1: Comparing Hypo+ISA model to the undrained cyclic triaxial tests using Ottawa F65 sand (q^{amp}=20 kPa, p_0=50 kPa).

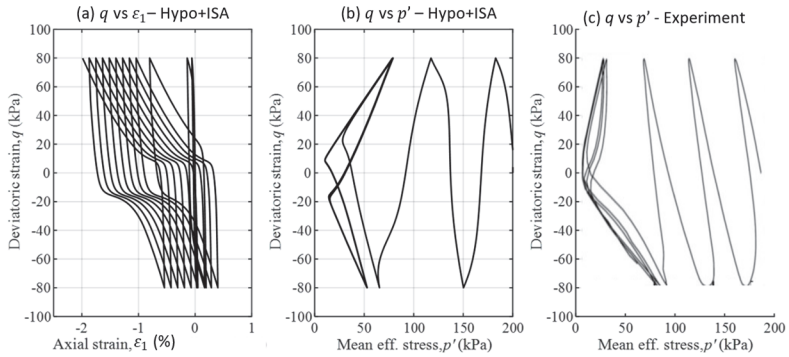

Figure 2: Comparing Hypo+ISA model to the undrained cyclic triaxial tests using Ottawa F65 sand (q^{amp}=80 kPa, p_0=200 kPa).

Figure 3 shows the results of pore pressure, u, mean effective stress, p', and excess pore pressure ratio, r_u, which is the ratio of excess pore pressure, Δu, to the initial mean effective stress, p'_0. The results are shown for a dense-of-critical void ratio e=0.45 (Figure 3a, 3b, 3c) and a loose-of-critical void ratio e=0.80 (Figure 3d, 3e, 3f). For dense soils in undrained conditions, the pore pressure decreases (Figure 3a), and the mean effective stress increases (Figure 3b). It is seen that pore pressure decrease manifests in a negative r_u, with a larger decrease in pore pressures at deeper depths. Overall, the Hypo+ISA constitutive model captures the soil's tendency to dilate at the dense void ratio. By contrast, for loose soils, the pore pressure increases (Figure 3d), and the mean effective stress decreases (Figure 3e). For depths between 1 to 6 m, the soil reaches zero mean effective stress with r_u equal to one, as represented in Figure 3f, corresponding to the almost

complete transfer of the load to the pore water (i.e., liquefaction). Stress oscillations are observed in the pore pressure after 6.5s (Figure 3d); these are attributed to cell-crossing occurrences that are not fully mitigated by the mixed-integration. The undrained system-level results can also be visualized for dense and loose sand in the effective stress path space (Figure 4). Loose sand exhibits stress paths that go left and towards the origin (i.e., tendency to contract and approach liquefaction). By contrast, dense sand exhibits stress paths that go right away from the origin.

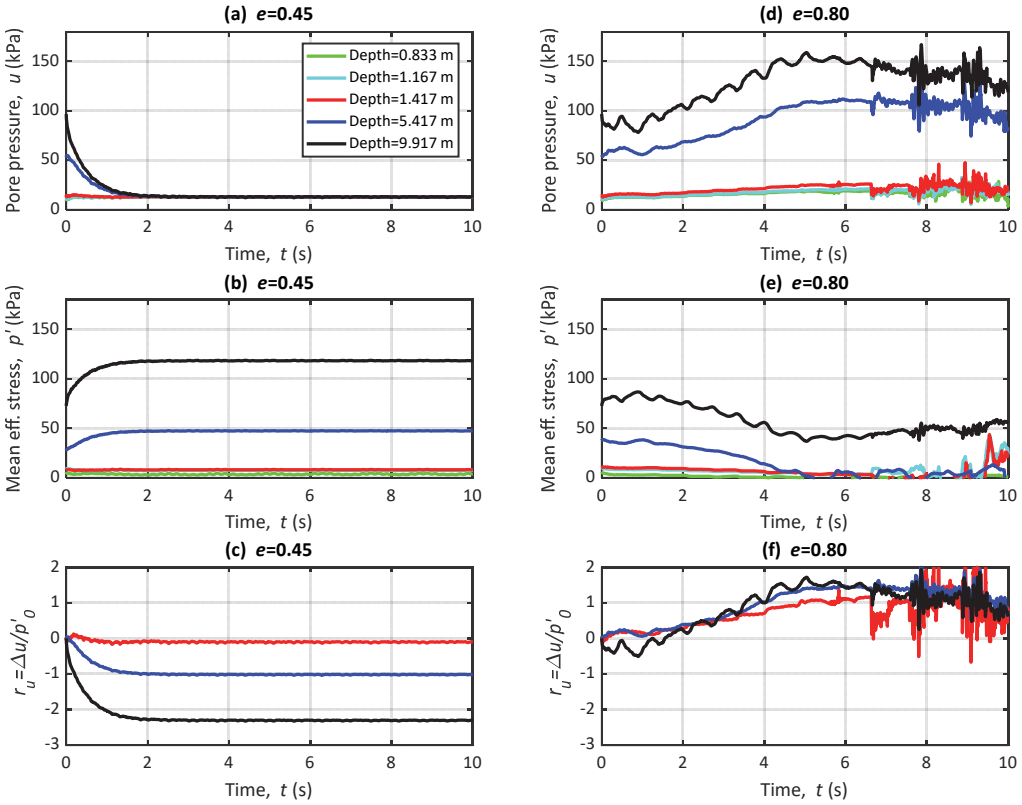

Figure 3. Pore pressure and mean effective stress history for different initial *e*.

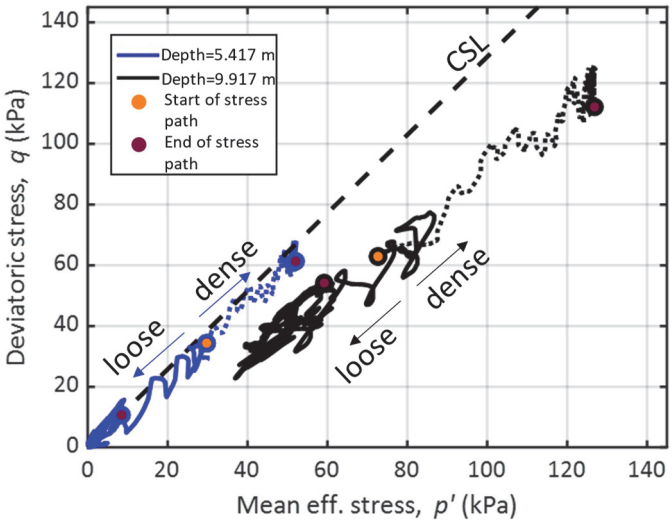

Figure 4. System-level Cambridge stress paths under undrained cyclic loading.

EARTHQUAKE-INDUCED LIQUEFACTION OF EARTHEN EMBANKMENT

This section aims to employ the framework in analyzing a theoretical small-scale geometry. The geometry is shown in Figure 5, where a 6 m high sand embankment overlies a 2 m linear-elastic foundation. The geometry was selected in such a manner to keep the slope close to the limit equilibrium to be able to showcase the effect of the initial void ratio on the post-failure consequences. The parameters used for the Hypo+ISA embankment are identical to the parameters used in the level-ground sand column example corresponding to Ottawa F65. The parameters used for the linear-elastic foundation are E'=10^6 kPa and ν'=0.33, corresponding to a stiff non-liquefiable layer. The values for G_s, ρ_w, and K_w are also identical to the sand in the level-ground soil column example for both materials herein. Three MPs are tracked at the center and the toes of the embankment corresponding to the regions with the largest and lowest initial mean effective stress, respectively.

The stress initialization was obtained as follows. The embankment was assumed to be fully saturated with the water table consistent with the slope geometry (Figure 5). Then, the effective stresses were initialized with a gravity loading quasistatic convergence step while keeping the pore pressure constant. During this process, the bottom boundary is assumed to be fully fixed, and the lateral sides are normally fixed.

For the dynamic calculation stage, the explicit generalized-α time scheme is activated with a bifurcation spectral ratio ρ_b=0.818. The selected time step is half of the critical time step as informed by the CFL condition (i.e., Courant number=0.5). The mechanical fixities were removed, and the non-zero kinematic boundary condition was applied at the base and periodic boundary conditions on the lateral sides. The applied ground motion accelerogram (Mw 6.61 San Fernando February 9, 1971, Maricopa array #2, H1 component, source-to-site distance R_{jb}=109 km) is obtained from the PEER database (Bozorgnia et al., 2014) and is applied using the non-zero kinematic boundary condition as a vertically propagating shear (SV) wave. The ground motion was baseline corrected to eliminate possible drift. This ground motion was also used in Alsardi and Yerro (2023) where the reader is referred to for more details.

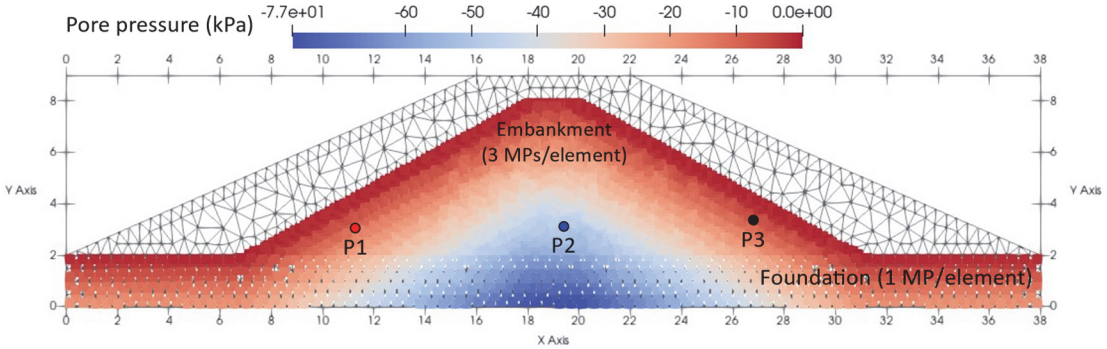

Figure 5. Background mesh, initial slope geometry, and hydrostatic pore water pressure.

Figure 6 shows the evolution of pore pressure and mean effective stress with time for void ratios ranging from 0.45 to 0.95 for the material points near the left toe (P1), center (P2), and right toe (P3) of the slope. The upper bound of the void ratio range was obtained as the minimum void ratio causing liquefaction to occur. When considering e=0.45, it is seen that pore pressures decrease and mean effective stresses increase, as shown in Figure 6a and 6d, respectively. Despite e=0.8 causing liquefaction in the previous column example, the system level response seen in Figure 6b

and 6e is similar to when e=0.45 was considered. By contrast, when considering e=0.95, the pore pressures tend to increase, and the mean effective stresses decrease as shown in Figure 6c and Figure 6f. The material points close to the toe reach mean effective stress of zero (i.e., liquefaction). Figure 7 shows the vertical displacement evolution with time at the center (P2) and toes of the embankment (P1 and P3); looser samples (Figure 7b and 7c) results in displacements that are one order of magnitude larger than the denser state (Figure 7a). Stress oscillation is observed in the pore pressures and the mean effective stresses, indicating the need for a more rigorous algorithm for improving volumetric locking and cell-crossing spurious artifacts, particularly when using advanced constitutive models. Figure 8 shows the final profiles for slopes with $0.45 \leq e \leq 0.95$, depicting that the vertical and horizontal displacements are larger for looser samples. In this particular case, the increase in vertical settlement is seen to be within the same order of magnitude as the increase in horizontal runout. Overall, the system-level response is captured satisfactorily in this small-scale MPM boundary value problem utilizing a simple undrained effective stress formulation with an advanced Hypo+ISA constitutive model. This indicates that the numerical framework is very promising for the large-strain simulation of the coseismic landslides capturing the hydromechanical aspects, triggering, and post-failure runout.

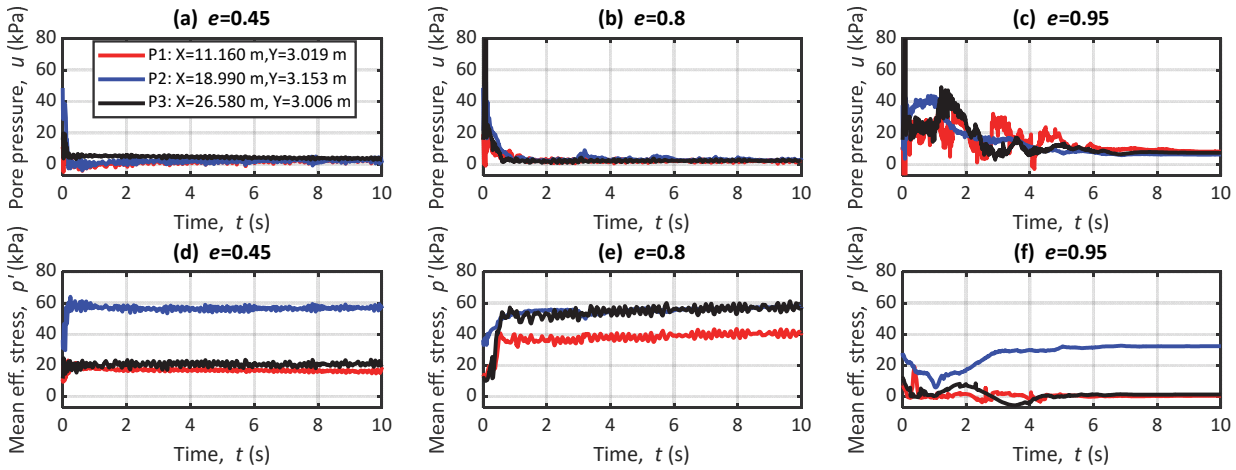

Figure 6. Pore pressure and mean effective stress for different slope initial e.

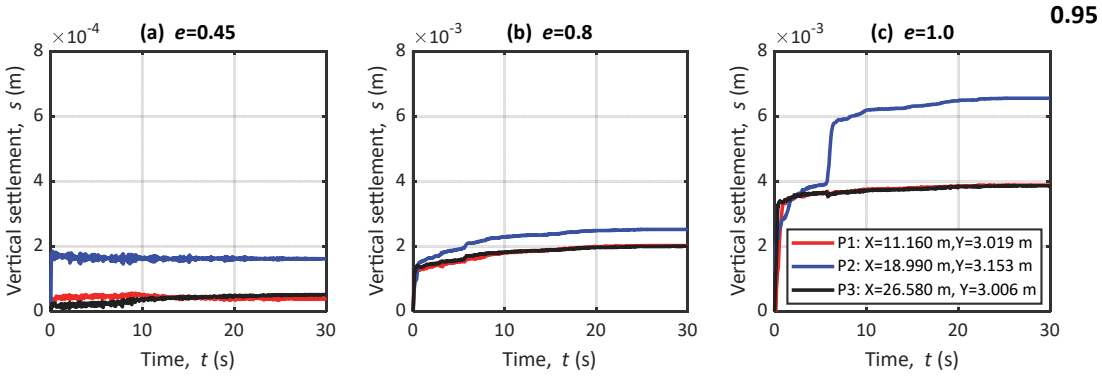

Figure 7. Vertical displacement history for different slope initial e.

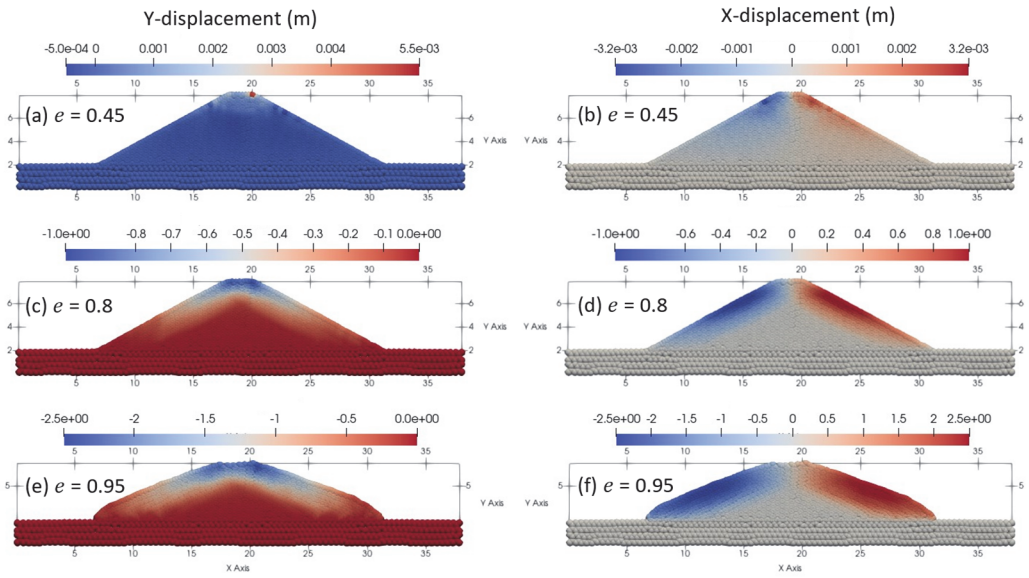

Figure 8. Final displacement contour plots for different initial void ratios ($0.45 \leq e \leq 0.95$).

CONCLUSIONS

In this paper, we used an MPM framework capable of inducing earthquake shaking and, for the first time, employed with the Hypo+ISA constitutive model. The system-level response was simulated using a level-ground sand column simulation and a small-scale sand embankment. As expected, the pore pressure behavior decreased when we considered a dense sample. By contrast, the pore pressure increased when we considered a loose void ratio. In loose sand, earthquake-induced liquefaction was exhibited, with the mean effective stress reaching almost zero. Further research is required to validate the applicability of constitutive models for large strains. Future steps would include comparing the system-level responses using a fully-coupled hydromechanical formulation against centrifuge tests with more complex stratigraphy and longer strong-shaking durations.

ACKNOWLEDGEMENTS

This research was partially funded by the National Science Foundation (NSF) (Grant No. CMMI-2211002). However, any opinions, findings, conclusions, or recommendations expressed in this material are those of the authors and do not necessarily reflect the views of the NSF.

REFERENCES

Al-Kafaji, I. K. J. 2013. Formulation of a Dynamic Material Point Method (MPM) for Geomechanical Problems. PhD thesis, Universitat Stuttgart.

Alsardi, A. and Yerro, A., 2021. Runout modeling of earthquake-triggered landslides with the material point method. In *IFCEE 2021* (pp. 21-31).

Alsardi, A. and Yerro, A., 2023. Coseismic site response and slope instability using periodic boundary conditions in the material point method. *Journal of Rock Mechanics and Geotechnical Engineering*, *15*(3), pp.641-658.

Alsardi, A., Copana, J. and Yerro, A., 2021. Modelling earthquake-triggered landslide runout with the material point method. *Proceedings of the Institution of Civil Engineers-Geotechnical Engineering*, *174*(5), pp.563-576.

Bozorgnia Y, Abrahamson NA, Atik LA et al. (2014) NGA-West2 research project. Earthquake Spectra, 30(3): 973–987

Bray, J.D., Macedo, J. and Travasarou, T., 2018. Simplified procedure for estimating seismic slope displacements for subduction zone earthquakes. *Journal of Geotechnical and Geoenvironmental Engineering*, *144*(3), p.04017124.

Dafalias, Y.F. and Manzari, M.T., 2004. Simple plasticity sand model accounting for fabric change effects. *Journal of Engineering mechanics*, *130*(6), pp.622-634.

Duque, J., Yang, M., Fuentes, W., Mašín, D. and Taiebat, M., 2021. Characteristic limitations of advanced plasticity and hypoplasticity models for cyclic loading of sands. Acta Geotechnica, pp.1-23.

Feng, K., Wang, G., Huang, D. and Jin, F., 2021. Material point method for large-deformation modeling of coseismic landslide and liquefaction-induced dam failure. *Soil Dynamics and Earthquake Engineering*, *150*, p.106907.

Fuentes, W. and Triantafyllidis, T., 2015. ISA model: a constitutive model for soils with yield surface in the intergranular strain space. *International Journal for Numerical and Analytical Methods in Geomechanics*, *39*(11), pp.1235-1254.

Fuentes, W., Mercado, V. and Lascarro, C., 2018. Evaluation of the ISA-hypoplasticity constitutive model for the LEAP-2017 project. In *Geotechnical Earthquake Engineering and Soil Dynamics V: Numerical Modeling and Soil Structure Interaction* (pp. 165-173). Reston, VA: American Society of Civil Engineers.

Fuentes, W., Wichtmann, T., Gil, M. and Lascarro, C., 2020. ISA-Hypoplasticity accounting for cyclic mobility effects for liquefaction analysis. *Acta Geotechnica*, *15*, pp.1513-1531.

Giridharan, S., Gowda, S., Stolle, D.F. and Moormann, C., 2020. Comparison of ubcsand and hypoplastic soil model predictions using the material point method. *Soils and Foundations*, *60*(4), pp.989-1000.

Kohler, M., Stoecklin, A. and Puzrin, A.M., 2022. A MPM framework for large-deformation seismic response analysis. *Canadian Geotechnical Journal*, *59*(6), pp.1046-1060.

Kularathna, S., Liang, W., Zhao, T., Chandra, B., Zhao, J. and Soga, K., 2021. A semi-implicit material point method based on fractional-step method for saturated soil. *International Journal for Numerical and Analytical Methods in Geomechanics*, *45*(10), pp.1405-1436.

Niemunis, A., 2008. *Incremental Driver User's manual*. Available from https://soilmodels.com/idriver/.

Poblete, M., Fuentes, W. and Triantafyllidis, T., 2016. On the simulation of multidimensional cyclic loading with intergranular strain. *Acta Geotechnica*, *11*(6), pp.1263-1285.

Sulsky, D., Chen, Z. and Schreyer, H.L., 1994. A particle method for history-dependent materials. *Computer methods in applied mechanics and engineering*, *118*(1-2), pp.179-196.

Von Wolffersdorff, P.A., 1996. A hypoplastic relation for granular materials with a predefined limit state surface. *Mechanics of Cohesive-frictional Materials: An International Journal on Experiments, Modelling and Computation of Materials and Structures*, *1*(3), pp.251-271.

Wichtmann, T., Fuentes, W. and Triantafyllidis, T., 2019. Inspection of three sophisticated constitutive models based on monotonic and cyclic tests on fine sand: Hypoplasticity vs. Sanisand vs. ISA. *Soil Dynamics and Earthquake Engineering*, *124*, pp.172-183.